Open access • Journal Article • DOI:10.1080/13621718.2017.1388995

# Effect of process parameters on the quality of aluminium alloy Al5Si deposits in wire and arc additive manufacturing using a cold metal transfer process



A. Gomez Ortega, L. Corona Galvan, Frédéric Deschaux-Beaume, Bachir Mezrag ...+1 more authors

**Institutions:** Centre national de la recherche scientifique

**Published on:** 19 May 2018 - Science and Technology of Welding and Joining (Taylor & Francis)

**Topics:** Arc welding, Welding, Process variable, Aluminium and Aluminium alloy

# Effect of process parameters on the quality of aluminium alloy Al5Si deposits in wire and arc additive manufacturing using a cold metal transfer process

Arturo Gomez Ortega, Luis Corona Galvan, Frédéric Deschaux-Beaume, Bachir Mezrag, Sébastien Rouquette

# Effect of process parameters on the quality of aluminium alloy Al5Si deposits in wire and arc additive manufacturing using a cold metal transfer process

A. Gomez Ortega, L. Corona Galvan, F. Deschaux-Beaume, B. Mezrag and S. Rouquette

LMGC, Univ. Montpellier, CNRS, Montpellier, France

**ABSTRACT**

A 3D print device using a cold metal transfer arc welding station to melt a metallic filler wire is developed to build aluminium part by optimising the process parameters. First tests achieved using standard pre-recorded process parameters allow to study the effect of the travel speed and the average welding power on the geometrical characteristics of mono-layer deposits and on walls built by layers superposition. Finally, a parametric study of the effect of each process parameter controlling the shape of the arc current or voltage and the filler wire feeding is carried out in order to try to improve the geometrical regularity of the deposits, and to better understand the effect of each parameter on the melting of the filler wire, its transfer on the support plate, and the geometry of the formed bead.

**KEYWORDS**

Additive manufacturing; aluminium alloy; cold metal transfer process; melting; optimisation

## Introduction

Additive manufacturing (AM) is a promising way to produce near-net shape metallic parts with complex geometries. It offers many advantages compared to machining processes, as reductions in the manufacturing lead-time and cost due to low material waste [1]. The AM denomination gathers various techniques for metallic parts manufacturing, which can be distinguished by the nature of the energy source allowing the metal deposit or densification, and by the form of the raw material [2]. Technologies based on powder bed melting, generally designated as selective melting technologies, using as heat source a laser [3] or an electron beam [4], allow to build parts with a good dimensional accuracy and low surface roughness. The direct energy deposition (DED) technologies, based on powder projection or filler wire melting, are more suited for the fabrication of bigger components due to its high deposition rate [5]. The heat source is often a laser beam [6], but can be also a plasma [7,8], or an electrical arc [9].

The wire and arc additive manufacturing (WAAM) is a DED additive manufacturing process derived from welding that uses a metallic wire as filler metal and an electrical arc as heat source to produce the wire melting [10]. It is a promising process, especially because of its high deposition rate, low-cost raw materials, low material losses, and to its capability to manufacture large parts [11]. Among the various arc processes that can be used for wire melting, the cold metal transfer (CMT) process seems to be one of the more suited for WAAM, thanks to its controlled current waveform and filler wire feeding that allow to obtain regular deposited weld bead [12]. This new process, derived from the conventional gas metal arc welding (GMAW) process, has been initially developed for minimising the welding heat input [13,14]. The CMT process couples a specific electrical current waveform, which allows to form a molten metal drop at the filler wire tip and to control its growth, to an alternating feeding of the filler wire, which allows the deposit of the metal drop with a minimal heat input [15]. The last developments of this process allows to create very complex current and voltage waveforms, coupling for instance current pulses forming axial transfer of small droplets through the electrical arc with metal transfer by short-circuit during the alternate feeding of the filler wire [16], or also an alternating current, inversing periodically the polarity of the filler wire [17]. However, due to the very large number of process parameters, optimising this process to obtain near-net shape parts by the addition of regular deposits is a very complex issue. Some recent studies have been devoted to the understanding of the effect of process parameters on the characteristics of welding or cladding [18–21]. Some authors also investigated the microstructure and mechanical properties of the welds obtained with the CMT process [22]. However, only few studies were dedicated to the optimisation of the CMT process parameters to improve the geometrical quality of the deposited layers to build metallic parts [12]. The geometrical accuracy of the process remains generally rather low, that constitutes one of its limitations, and finishing machining is required when a good dimensional accuracy is needed. One of the more promising potential applications of the process, considering its

specific characteristics, is the building of shell shape structures of thicknesses between about 2 and 10 mm, which correspond to the thicknesses of the deposited beads.

The present work is a contribution to the improvement of the knowledge of the effect of CMT process parameters on the geometrical characteristics of aluminium deposited beads, in view of building shell shape aluminium parts.

## Experimental details

### 3D print device

A dedicated 3D print system has been developed for this study. It is composed of a three axis worktable and a fixed CMT welding torch (Figure 1). The work-table can be translated thanks to step-by-step motors with an accuracy of 1 $\mu$m in the horizontal ($XY$) plane and 2.5 $\mu$m on the vertical axis $Z$, allowing the build-ing of parts of 350 × 350 × 300 mm$^3$ maximal size. The travel speed of the worktable on the $XY$ plane can reach 5000 mm min$^{-1}$. The 3D print is piloted using the free software Repetier, which allows to import 3D models, to slice the 3D shape in layers of given thickness, and to pilot the 3D printer, thanks to an Arduino control board.

### Heat source and material

A CMT Advanced welding source of Fronius is used to control the melting and the feeding of the 1.2 mm diameter aluminium wire. The filler wire material is an Al–Si alloy containing about 5% of Si (ER4043 according to AWS, Table 1). A 6 mm thick plate of 1050 aluminium alloy is used as substrate. The CMT process is used in its 'conventional' configuration, i.e. without superposing pulsed current or alternating current on the CMT

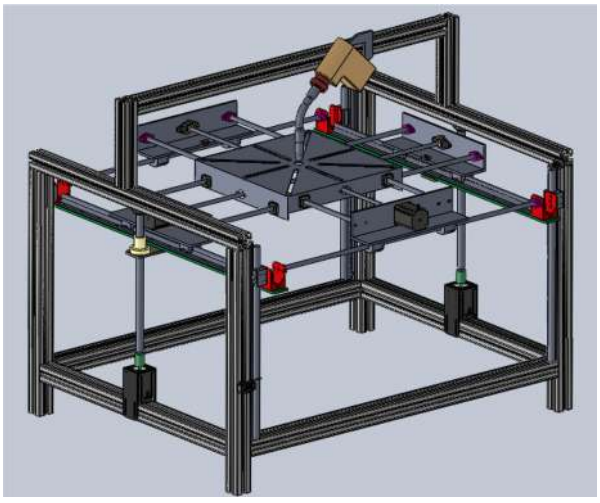

**Figure 1.** Representation of the 3D print device developed for the study.

**Table 1.** Composition of the ER 4043 (AlSi5) filler wire.

| Element | Si | Mn | Mg | Cu | Fe | Zn | Ti | Al |
|---|---|---|---|---|---|---|---|---|
| Wt-% | 5 | < 0.05 | < 0.05 | < 0.05 | < 0.40 | < 0.10 | < 0.20 | Solde |

current waveform. This configuration requires, however, the combined choice of 15 main parameters to control the melting of the filler wire tip and its deposit on the form of molten drops. These parameters can be classified into three classes, the first ones relative to the ignition phase, the second to the deposit phase, and the last ones to the end phase of the deposit. In this study, only the effect of the second parameters class is investigated, the others being chosen equal to the recommended values of the process for welding with Al-Si filler wire. So only 8 parameters controlling the deposit are taken into account. Figure 2 resumes the signification of these parameters, controlling the current and voltage waveforms, or the feeding rate of the filler wire. Parameter (11) controls the value of the 'Boost current' $I_{boost}$ (A) of the plasma phase, which allows the melting of the wire tip. Parameter (12) controls the duration $t_{boost}$ (ms) of this boost phase. Parameter (6) controls the value of the 'Wait current' $I_{wait}$ (A), following the boost phase until the dipping of the wire electrode into the weld bead, creating the arc extinction and the beginning of the short-circuit phase. Parameter (7) controls the feeding rate of the wire $V_d$ (m min$^{-1}$) at the end of the boost phase until the dipping of the wire electrode into the weld bead. Parameter (8) controls the value of the current $I_{sc}$ (A) during the short-circuit phase. Parameter (9) controls the linear current rise rate $D_{boostup}$ (A ms$^{-1}$) at the start of the boost phase. Parameter (10) controls the non-linear current rise rate $T_{boostup}$ (ms) at the start of the boost phase. Parameter (13) controls the linear rate of current decrease $D_{boostdown}$ (A ms$^{-1}$) following the boost phase. Finally, parameter (14) controls the non-linear current decrease rate following the boost phase. This last parameter is not displayed for the CMT cycles used in this study.

### Process analyses

In order to record the current and voltage waveforms during all the deposit, the CMT process is instrumented with a Hall effect based current transducers (LEM LT 505-S) to measure the process current, and the voltage is measured between the support plate of the deposits and the contact tip of the welding torch, both with a frequency of 80 kHz. In order to observe *in situ* the melting of the filler wire and the metal transfer, video recordings of the filler wire tip are also made with a high speed camera (Phantom ir300) at 5000 images per second. To partly eliminate the arc radiation, a 808 nm interferential filter is placed on the camera, and coupled to a laser diode to light the tip of the filler wire.

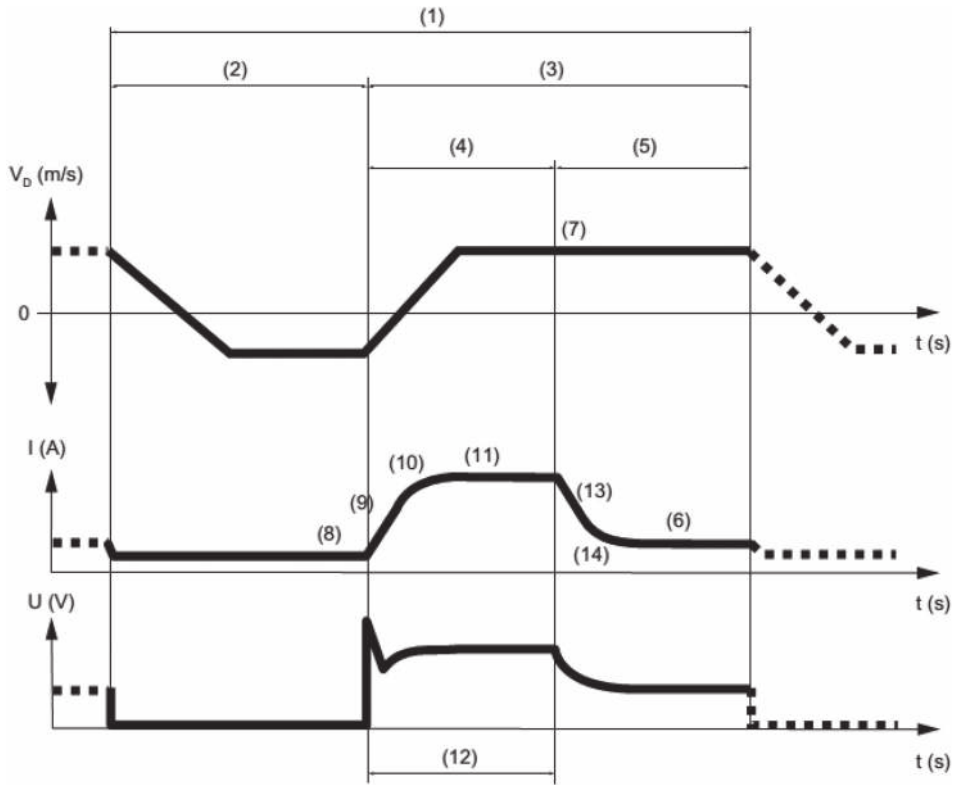


**Figure 2.** Schematic representation of the current (*I*) and voltage (*U*) waveforms and of the feeding rate ($V_d$) variation during a CMT cycle. (1) CMT cycle time, (2) short-circuit phase, (3) plasma phase, (4) boost phase, (5) wait phase.

The experimental tests consist to deposit linear beads of about 100 mm length with controlled CMT parameters to form monolayer beads or multilayer walls by adding up to 100 layers. In order to analyse geometrical parameters of the deposited layers, samples are scanned using a Breuckmann 3D scan to obtain STL format files, which are then treated thanks to the Geomagic commercial software, and a dedicated Python routine. Geomagic software is used to calculate the total volume of the deposit and to deduce the total deposited mass, supposing the aluminium density equal to 2700 kg m$^{-3}$. Figure 3 shows an example of STL file created from the 3D scan of a multilayer deposit, and the associated volume calculated with Geomagic. The developed Python routine consists to import the STL file, to separate the deposit from the support, and then to extract the bead contour on 50 transverse cross sections of the centre part of the deposit, separated each one of 0.1 mm, in order to measure the maximal height and the contact angle of each section (Figure 4(a,b)). The average height and contact angles of the bead and the standard deviations are then computed from the measures on theses 50 sections. The bead width is measured from the bead contour on sections parallel to the plan of the support plate (Figure 4(c)). As the contact angle A between the support and the bead varies considerably according to the process parameters, from about 70° when the bead does not spread to the plate, to more than 140°, the monolayer width are measured for all the bead on one plan,

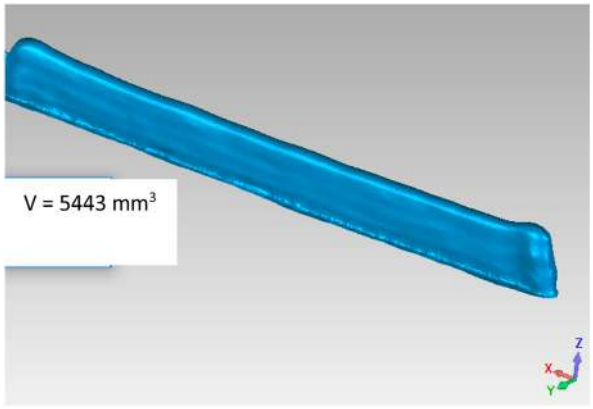


**Figure 3.** STL file obtained from the 3D scan of a multilayer deposit.

at a distance of 0.5 mm from the plan of the support plate surface (Figure 4(a)). The average and standard deviation of the width are then computed from the bead contours extracted on this plan.

## Preliminary results with standard process parameters

Firsts deposit tests are carried out using 'standard' process parameters pre-recorded in the welding station for an AlSi5 filler wire (Table 2), and various travel speeds between 150 and 2400 mm min$^{-1}$. The average power is given as an indicative value, as it can change slightly with the travel speed. Note that for this energy range,

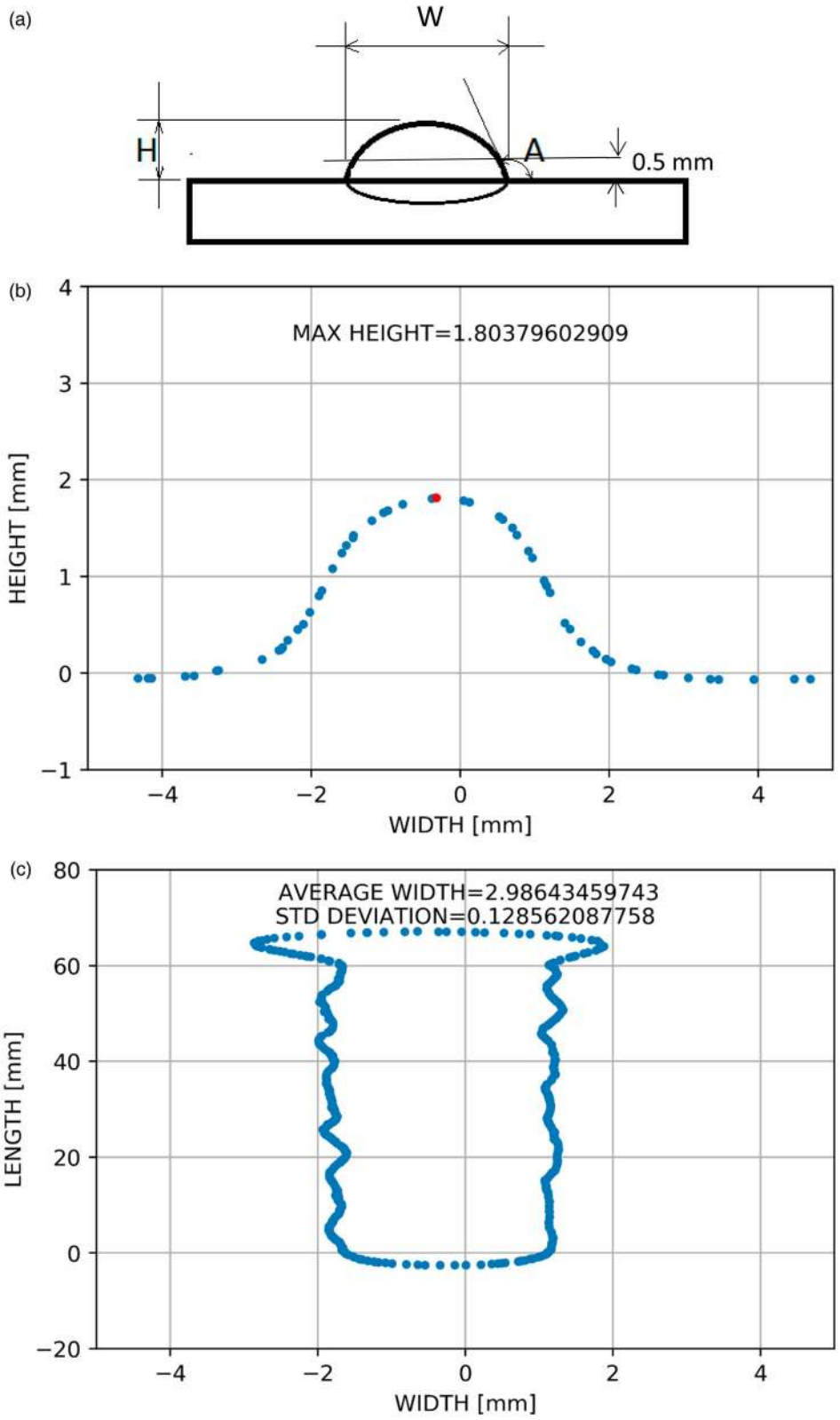


**Figure 4.** (a) Measures of the width W, height H and contact angle A on transverse and longitudinal sections of the beads extracted from the STL file, (b) bead contour extraction on a transverse section, and (c) bead contour extraction from a longitudinal section on the plane parallel to the plate surface at 0.5 mm from this plan.

**Table 2.** Pre-recorded process parameters of the CMT, and associated average power.

| | $I_{wait}$ (A) | $V_d$ (m min$^{-1}$) | $I_{sc}$ (A) | $D_{boostup}$ (A ms$^{-1}$) | $T_{boostup}$ (ms) | $I_{boost}$ (A) | $t_{boost}$ (ms) | $D_{boostdown}$ (A ms$^{-1}$) | Average power (W) |
|---|---|---|---|---|---|---|---|---|---|
| P4 | 50 | 20 | 40 | 300 | 0.1 | 150 | 2 | 300 | 708 |
| P5 | 70 | 25 | 40 | 300 | 0.1 | 150 | 2 | 300 | 1039 |
| P6 | 70 | 35 | 40 | 300 | 0.1 | 150 | 5 | 300 | 1470 |
| P7 | 70 | 37,5 | 40 | 300 | 0.1 | 135 | 9,5 | 300 | 1666 |

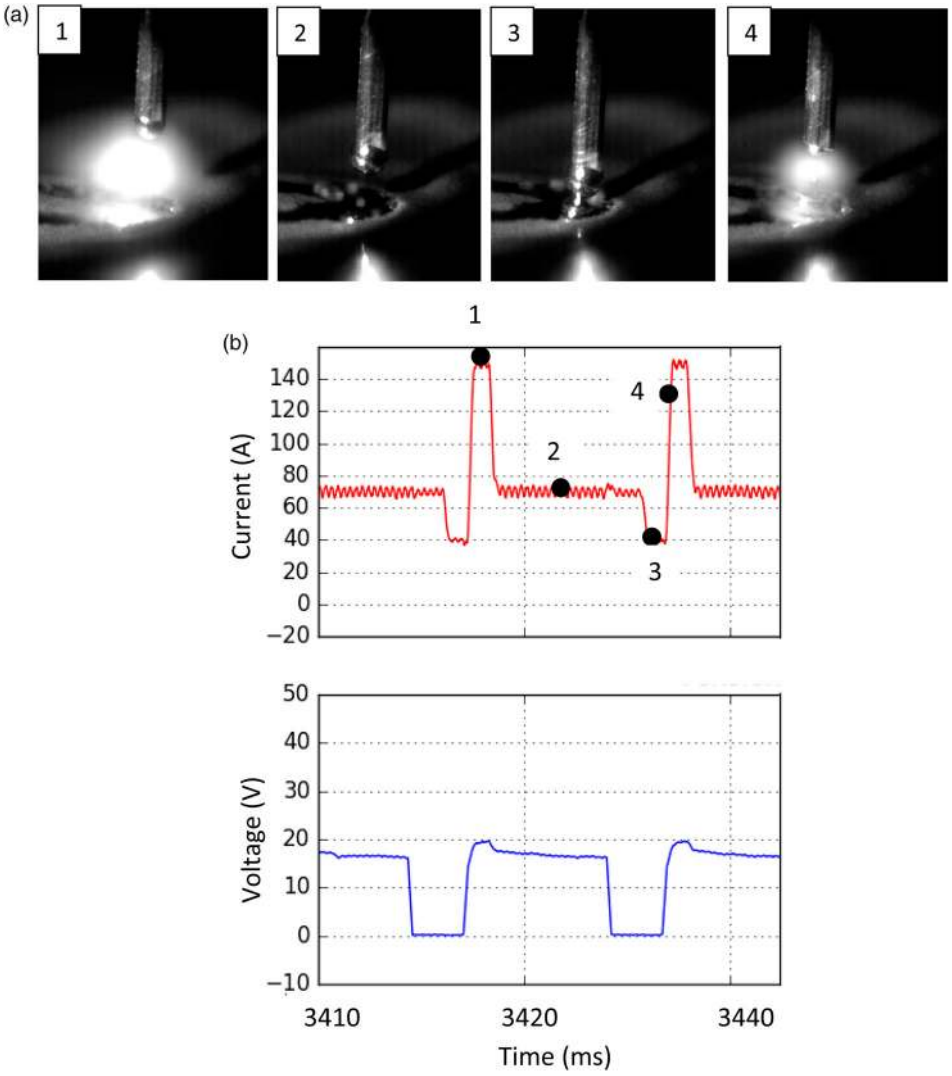


**Figure 5.** (a) High speed camera images of the CMT transfer cycle: melting of the wire tip during the boost phase (1), feeding of the wire during the wait phase (2), short-circuit (3), detachment of the deposited drop at the end of the short-circuit phase (4), and (b) current and voltage waveforms.

only four process parameters are changed in the pre-recorded parameters to modify the average power. Two kind of deposit are achieved: monolayer deposits of about 100 mm long, and multilayer deposits, superposing layers to form a wall.

### *Analyse of the metal transfer for a standard CMT cycle*

The synchronisation of high speed camera and current and voltage recording during a deposit allows to understand the heating mechanisms and the drop transfer during a typical CMT cycle. Parameters P5 are chosen as reference for this analysis (Figure 5). In a first step, the filler wire tip is heated up to its melting by the condensation heat of electrons crossing the electrical arc through the anode during the 'boost' of the plasma phase, corresponding to a current pulse of intensity $I_{boost}$ and duration $t_{boost}$ (Figure 5(a1)). The global heating of the wire tip then increases with the total power produced during this phase, i.e. with the increase of $I_{boost}$ or $t_{boost}$. However, a significant part of the condensation heat is lost due to the metal vaporisation that consumes a part of the heat, and to the heat conduction in the filler wire and the welding gun. So an increase in $t_{boost}$ or $I_{boost}$, by increasing the maximal temperature of the wire tip and/or the duration of the thermal transfer, can promote these losses and decrease the heat efficiency for the filler wire melting. During the 'wait' phase, the filler wire is fed towards the support plate, or the building part for a multilayer deposit (Figure 5(a2)). However, the arc plasma transporting electrons, continues to promote or maintain the heating of the filler wire tip. This heating increases with the current value of the wait phase. If this value is too low, the wire tip can cool down and solidify, preventing the transfer of molten drop. At the opposite, if its value is too high, it can produce an excessive growth of the molten drop at the wire tip and its detachment, producing risk of spatter. The duration of this

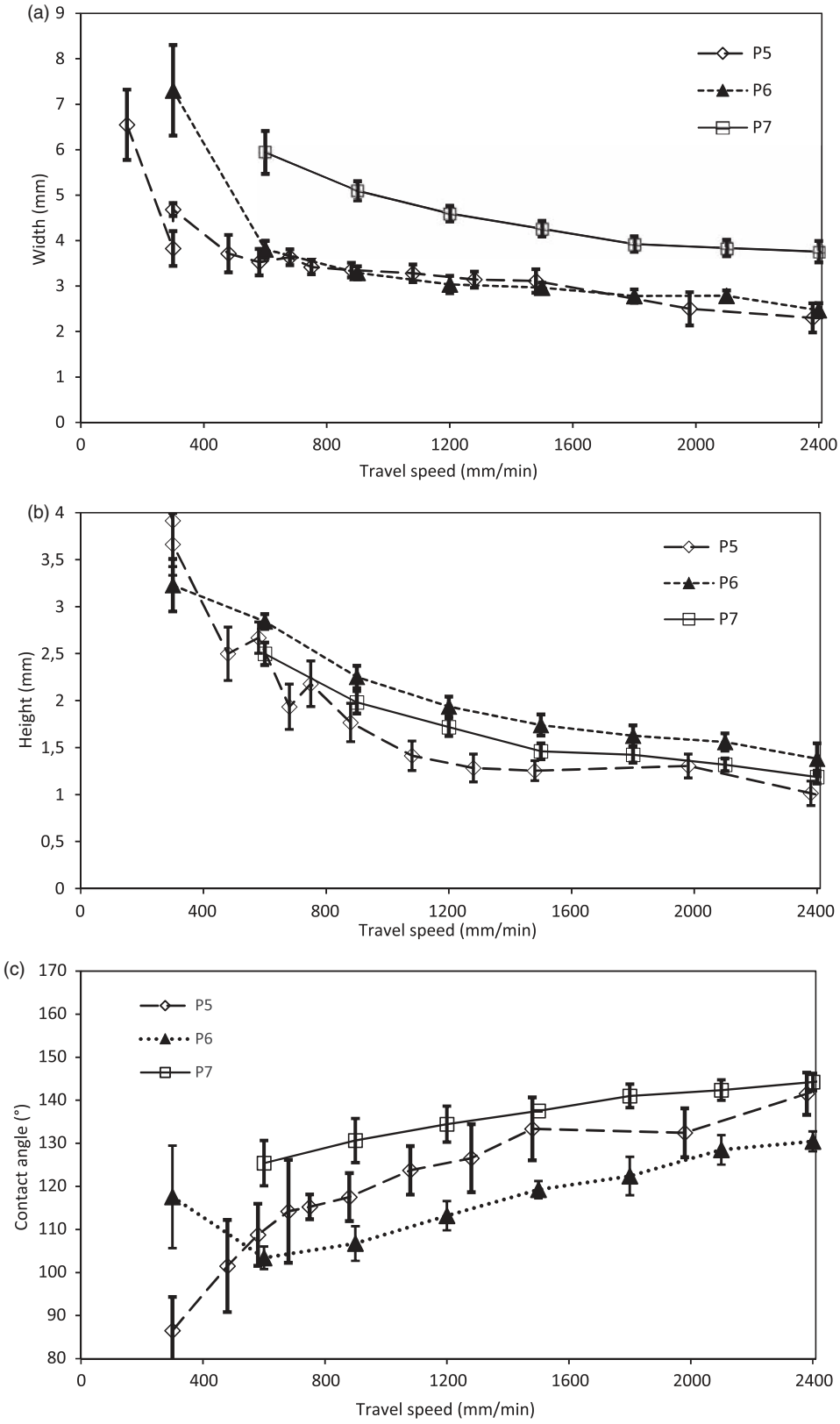


**Figure 6.** (a) Width, (b) height and (c) contact angle of monolayer deposits versus travel speed for the various parameters set.

phase is determined by the $V_d$ parameter, which controls the feeding speed, so an increase of this parameter decreases the duration of this phase. Finally, the filler wire is retracted, and the drop is deposited and wet the substrate (Figure 5(a3,4)). This wetting phase is very important because it determines the geometry of the solidified bead. In general, due to the high frequency of the short-circuit during the process, the molten part is composed of a melt of several drops deposited during successive short-circuits, but the number of these molten drops decreases with the travel speed, and a discontinuous bead constituted of separated solidified

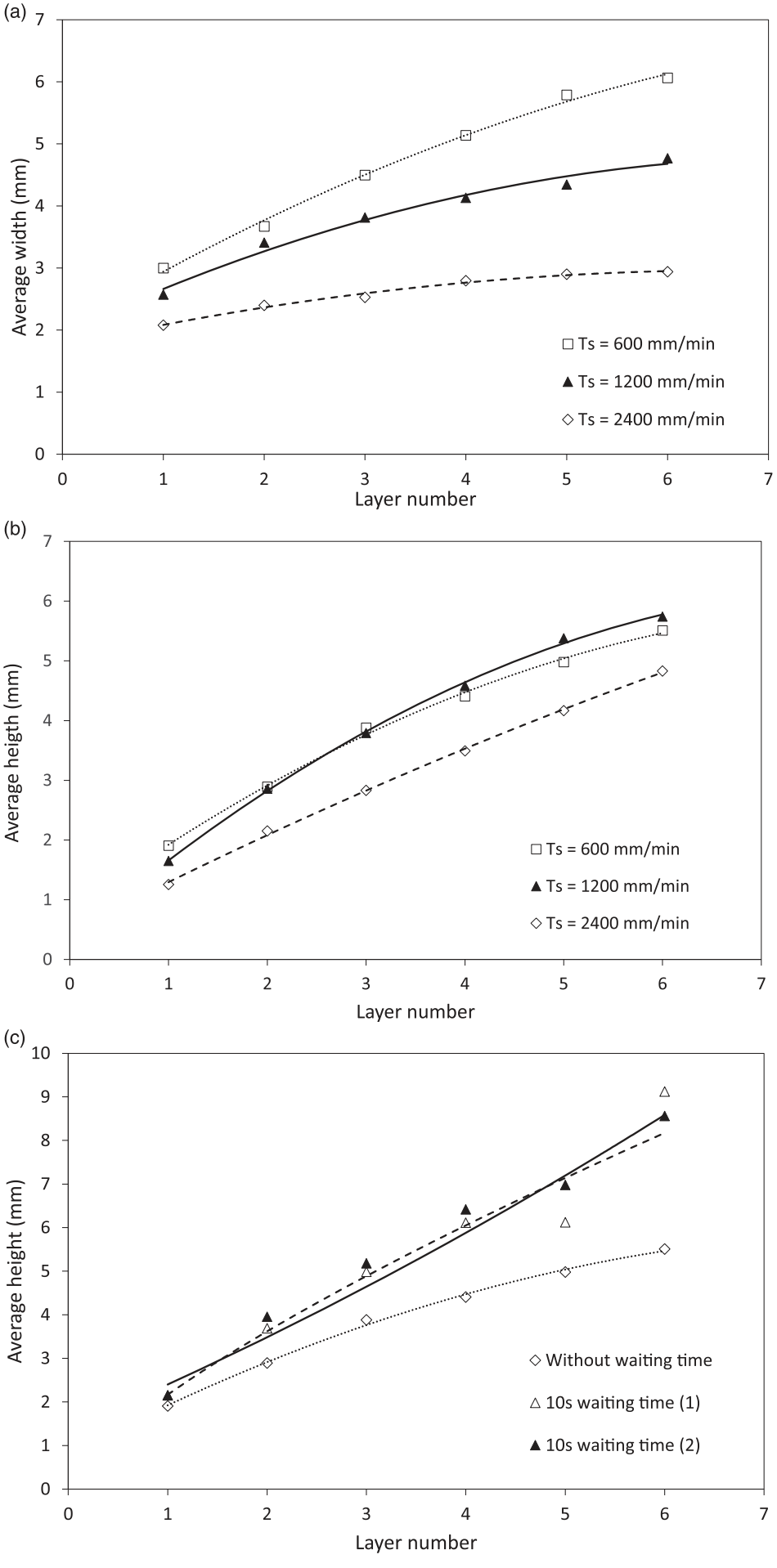


**Figure 7.** Evolution of the average width (a) and height (b, c) with the layer number for the parameters set P5.

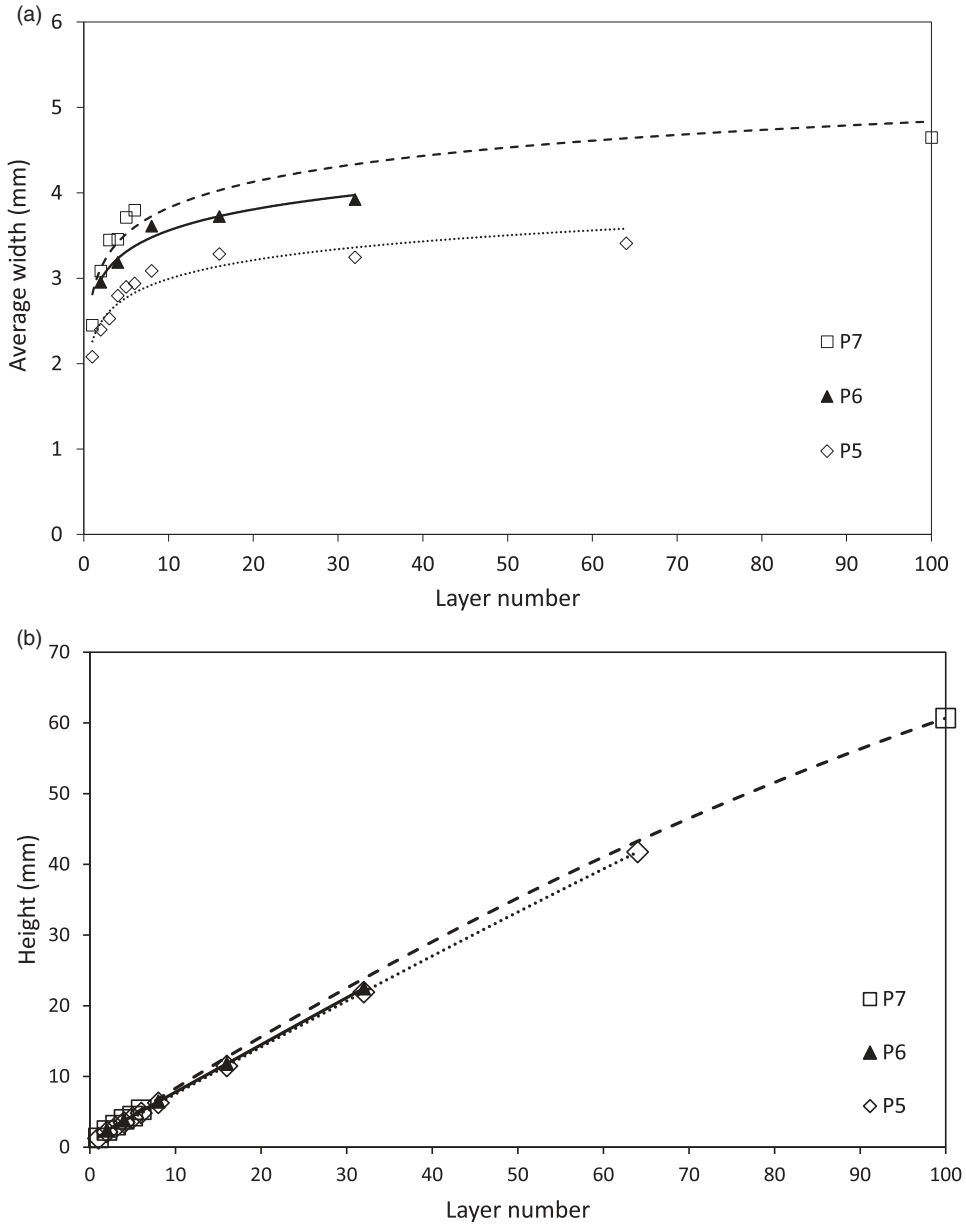


**Figure 8.** Evolution of the average width (a) and height (b) with the layer number for a travel speed of 2400 mm min$^{-1}$.

drops can be formed if this speed is too high. The wetting depends on many factors as the composition of the welding gas, the temperature of the molten phase and of the substrate, and can be disturbed by mechanical forces as arc pressure or gas flow. In particular, if the current pulse is high, the arc pressure increases, causing deformation of the molten pool. The liquid flow into the weld pool and the viscosity of the liquid can also have an influence on the geometry.

### *Monolayer deposits*

The first parameters set P4, corresponding to an average electrical power of about 700 W, forms a discontinuous deposit even for the lowest travel speed. This indicates a minimum power included in the 700–1000 W range is required to allow a sufficient melting of the wire tip to form a continuous deposited bead.

For the three other parameters set (P5 to P7), continuous deposits can be formed, whatever the travel speed of the worktable (Figure 6). However, the deposited bead is very irregular when the travel speed is below 300 mm min$^{-1}$ for parameters P6 and below 600 mm min$^{-1}$ for parameters P7. The maximal travel speed is limited to 2400 mm min$^{-1}$, because above this value, the deposits become less regular and more discontinuous, especially for parameters P5. When the travel speed increases from 150 to 2400 mm min$^{-1}$, the bead width decreases and then stabilises to a value between 3 and 4 mm in the tested speed range. Conversely, the height continuously decreases and the contact angle increases, indicating a better spreading of the deposited metal when the travel speed increases. The standard deviation for the contact angle remains rather constant when the speed increases, meaning the wetting of the liquid metal on the support plate remains

**Figure 9.** Aluminium wall built with 100 layers deposited using parameter set P5.

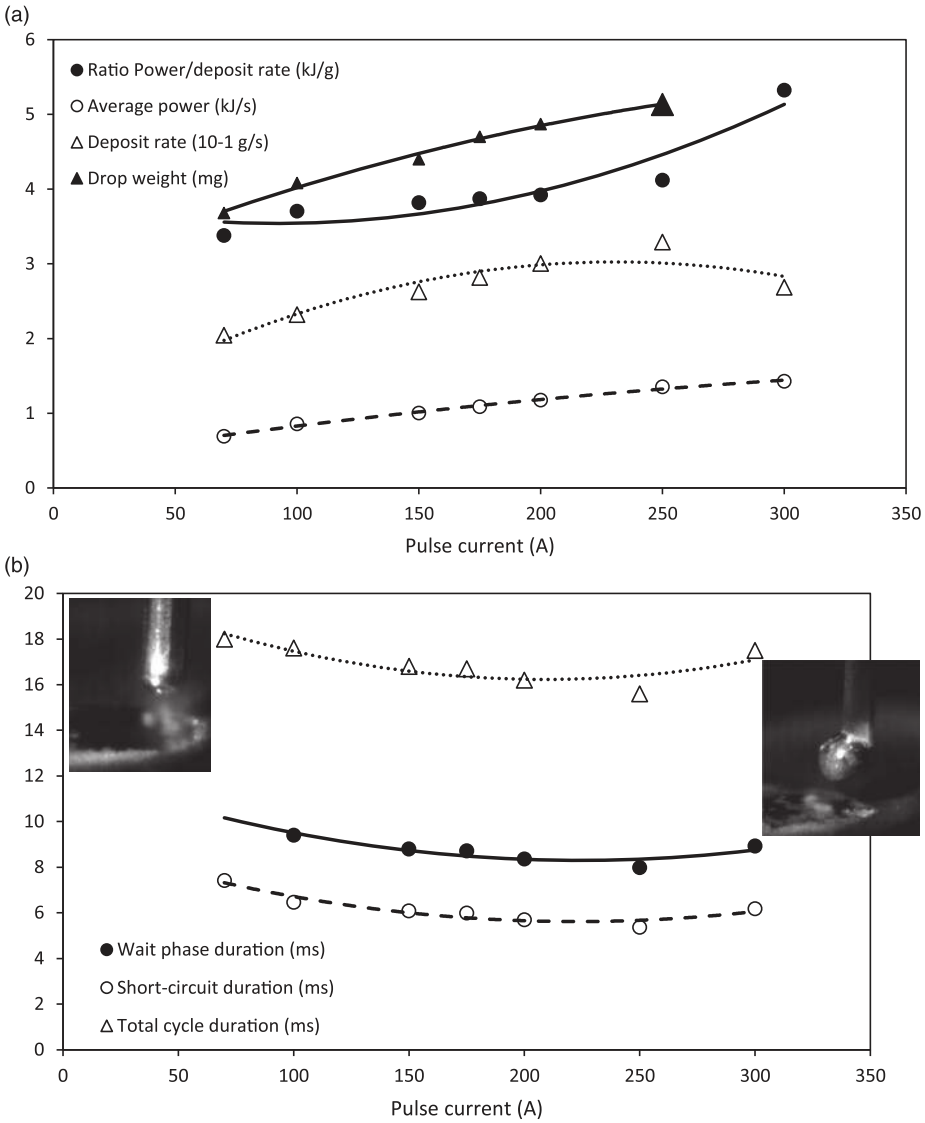


**Figure 10.** Effect of the pulse current (a) on the characteristics of metal transfer and heat transfer, and (b) on the average durations of the various phases of the CMT cycle.

regular up to 2400 mm $min^{-1}$, despite the support heating is reduced. Note that the standard deviation for the contact angle is higher for parameters P5, indicating a too low average power is detrimental for a regular wetting. The standard deviation for the averages width and height are also rather important, of about 0.2 mm

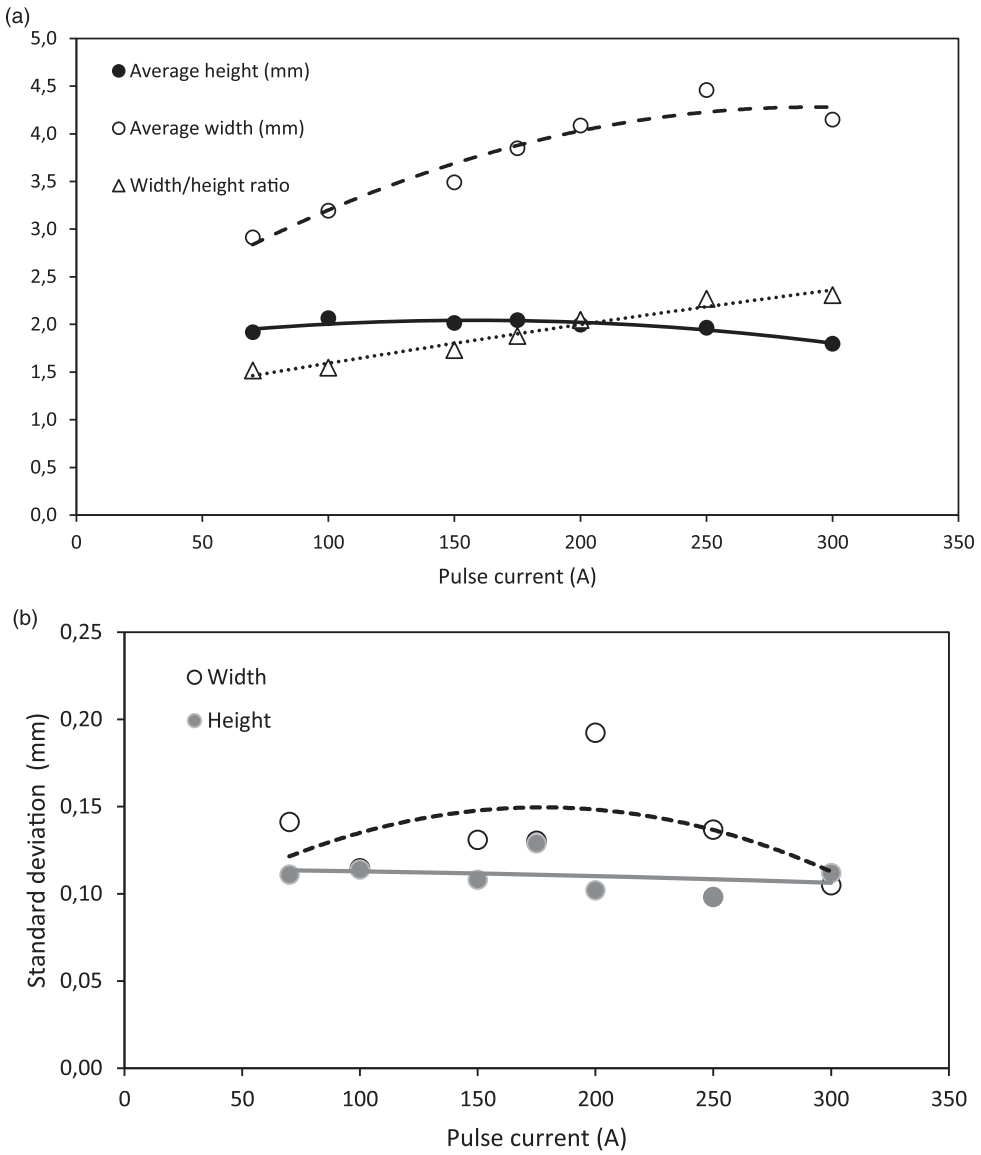


**Figure 11.** (a) Evolution of the average width and height of the deposits, and (b) of their standard deviation versus the pulse current

for the width and 0.1 mm for the height, which could limit the dimensional accuracy of the shell structures built with this process.

### *Multilayer deposits*

The first results of multi-layer deposits show the heat power has to be minimised and the travel speed increased otherwise the width of the deposits strongly increases with the layer addition due to heat accumulation and re-melting of the previous layers (Figure 7(a)). Conversely the height added at each layer decreases (Figure 7(b)), which is a handicap for additive manufacturing because the thickness of each new deposited layer should be then adapted. The addition of a waiting time between two layers reduces the width increase, but for practical reasons this waiting time could not exceed few seconds, otherwise the manufacturing time will be too long. Finally, a waiting time of 10 s between two layers has been retained as a good compromise to obtain acceptable manufacturing time with a sufficient cooling of the material between two layers, limiting the width increase and giving a quasi linear height increase with the layer addition (Figure 7(c)). The objective being to identify process parameters allowing the manufacture of an aluminium part by CMT additive manufacturing without changing process parameters, except the travel speed, the lowest power parameters set P5 has been retained. These process parameters allow to build multilayer walls with a stabilisation of the average width at around 3.5 mm when the maximal travel speed of 2400 mm $min^{-1}$ is used (Figure 8(a)), and the height of the wall then increases quasi-linearly with the layer number (Figure 8(b)). The other parameters set P6 and P7 give thicker walls, and the height increase with the layer number is not perfectly linear. Finally, a wall constituted of 100 layers with a constant thickness has been built using parameters P5 and a travel speed of 900 mm $min^{-1}$ for the first layer, progressively increased during the sixth first layers up to 2400 mm $min^{-1}$ (Figure 9). The standard deviation of the wall thickness measured was however

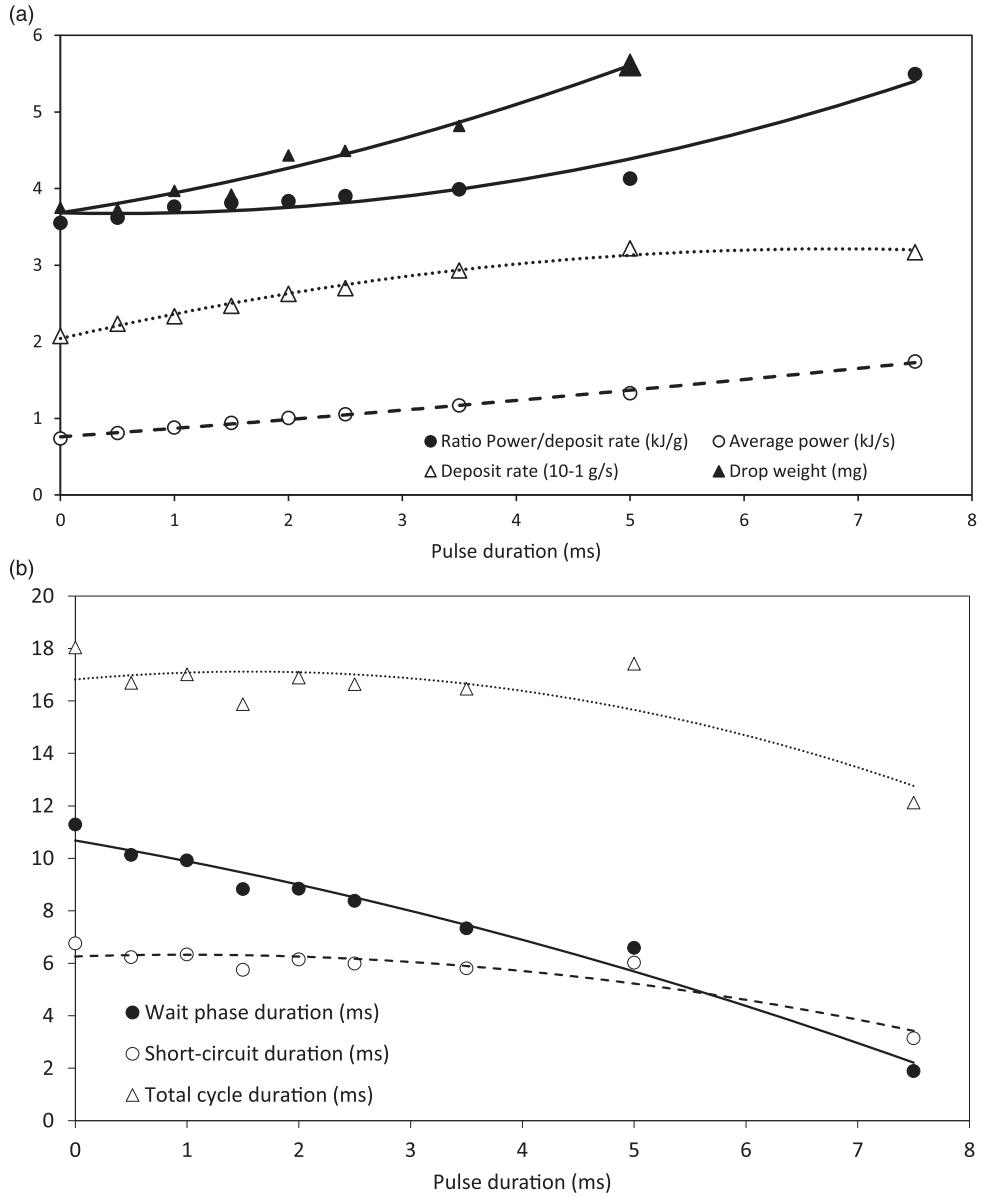


**Figure 12.** Effect of the pulse duration on (a) the characteristics of metal transfer and heat transfer, and (b) the average durations of the various phases of the CMT cycle.

rather high, with a value of more than 0.3. This low geometrical accuracy is unacceptable for most applications, and requires to deposit an excess of material, that have to be later removed by machining. In order to limit these costly operations, the geometrical accuracy of the deposited layers has to be improved. The last part of the study aims to investigate the effect of changing the main process parameters on the geometrical characteristics of the deposits, in view of optimise these parameters for obtaining a better geometrical accuracy.

## Optimisation of process parameters

In order to improve the geometrical quality of the deposits, but also to better understand the effect of each process parameter on the heating of the filler wire and the metal transfer to form a deposit, the effect of each parameter is studied by varying its value from the pre-recorded value of set P5. Several results are considered in order to investigate the effect of the modified parameter: the energy evolution corresponding to each phase of the CMT cycle; the duration of each phase and the short-circuit frequency, corresponding also to the frequency of drop deposit; the mass deposited par second and per short-circuit, and of course the geometrical parameters of the deposited bead, height, width and standards deviations. The mass deposited to each short-circuit, i.e. the drop weight $Wd$, is computed from the total volume $V$ of the deposit and the number of short-circuits Nsc numerically computed from the voltage record (each short-circuit being automatically detected and counted when the voltage value decreases to around zero) using the following relation:

$$Wd = \frac{\rho V}{\mathrm{Nsc}} \tag{1}$$

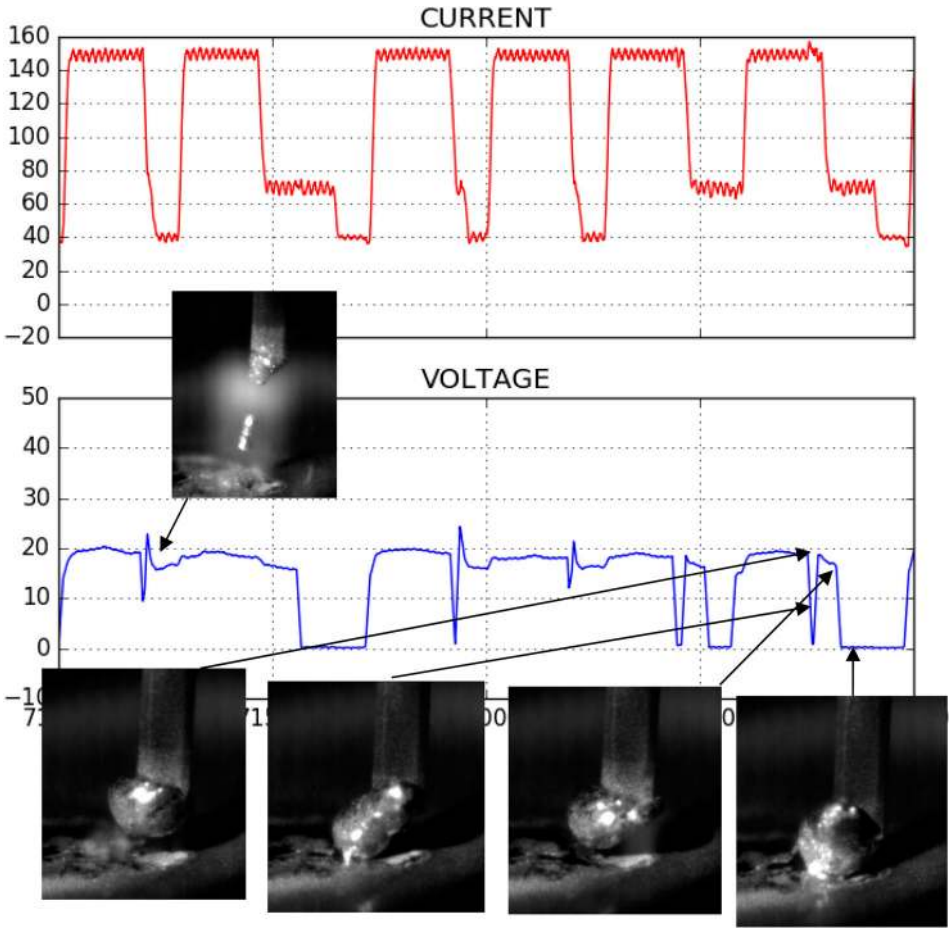


**Figure 13.** Metal transfer instabilities observed for a high pulse duration.

where $\rho$ is the material density supposed equal to 2.7 g cm$^{-3}$

Only six parameters are considered, supposed the more important for the stability of the transfer cycle.

### *Parameters controlling the 'boost phase'*

The boost phase is of great importance on the CMT cycle, because it controls the melting of the wire tip. Three main parameters can pilot this phase: the pulse current $I_{boost}$, the pulse duration $t_{boost}$, and the current down rate at the end of the pulse $D_{boostdown}$ (Figure 2). Varying the pulse current changes the heat energy produced by the boost phase, and then the volume and weight of the molten drop at the wire tip for each boost phase (Figure 10(a)). An increase of this parameter then increases the deposit rate and the average power P of the CMT cycle, numerically computed from the voltage and current records according to the following formula:

$$P = \frac{1}{\mathrm{tf}} \int_0^{\mathrm{tf}} UI\mathrm{d}t \qquad (2)$$

where $U$ and $I$ are, respectively, the instantaneous voltage and current, and tf is the total duration of the deposit.

The ratio between the energy and the deposited mass increases also with the pulse current, indicating the molten drop could reach a higher temperature. As a consequence, the duration of the wait phase before the short circuit is slightly reduced when the current pulse increases (Figure 10(b)), because the pendant drop at the wire tip is larger, and then enter more rapidly in contact with the bead. The short circuit period is also slightly reduced, probably due to the higher temperature of the deposited drop, which have a lower viscosity favouring the drop detachment. The cycle frequency then slightly increases when the pulse current increases, from about 57 s$^{-1}$ for a pulse current of 100 A to about 64 s$^{-1}$ for 250 A. Note that for a pulse current higher than 250 A, the deposit rate decreases (Figure 10(a)), probably due to an excessive vaporisation of Al and to spalling observed on the plate. Indeed, this high current creates drop detachment due to high Lorentz forces, which are projected out of the bead. Owing to the larger volume of deposited molten metal and to its higher temperature, the wetting on the substrate plate is improved, as indicated by the higher width/height ratio of the deposited bead (Figure 11(a)). However, if the geometrical aspect of the bead changes with the pulse current, the standard deviation computed for the height and the width of beads does not change drastically (Figure 11(b)). This parameter characterising the geometrical stability of the deposited bead remains between 0.1 and 0.15 mm when the pulse current is in

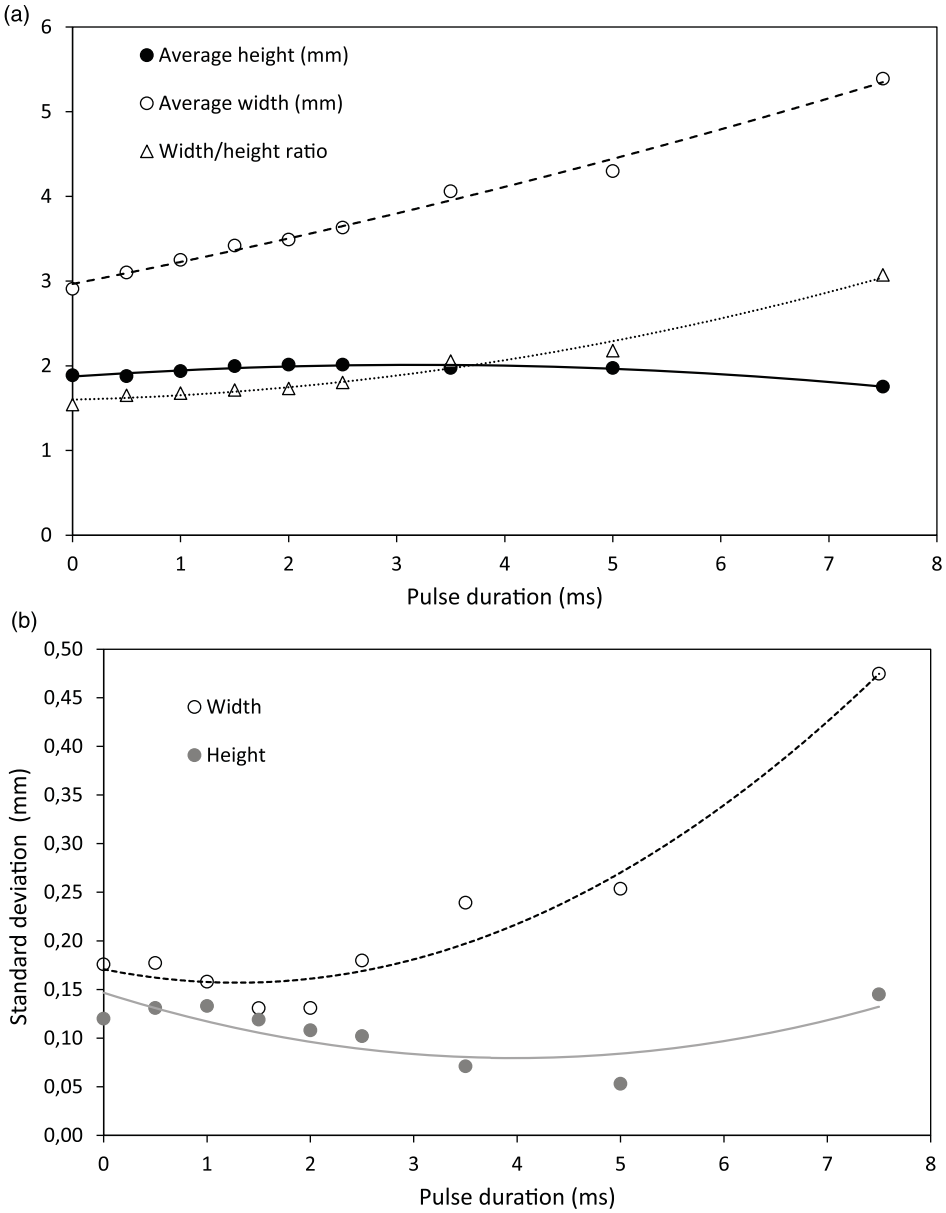


**Figure 14.** (a) Evolution of the average width and height of the deposits, and (b) of their standard deviation versus the pulse current.

the 70–175 A range, whereas the computed width standard deviation seems to slightly increases for higher current (Figure 11(b)).

The increase of the pulse duration also increases the heating of the filler wire tip and then its melting rate (Figure 12(a)). The average power, the deposit rate but also the ratio energy/deposit weight increase on the same way. As a result, the geometry of the deposit changes, increasing its width with a rather constant height, due to a better spreading of the molten metal on the support when the pulse duration increases (Figure 14(a)). As for the current pulse, an increase of this parameter decreases slightly the durations of the wait and short-circuit phases, producing an increase of the frequency of droplets detachment on the substrate (Figure 12(b)). Note that when the parameters $I_{boost}$ or $t_{boost}$ are too high, the periodic transfer of the drop during each short-circuit typical of the CMT transfer is disturbed, due to the detachment of droplets during the wait phase before the contact of the filler wire tip with the substrate, or to the oscillation of large droplets at the wire tip (Figure 13). This perturbation of the CMT transfer cycle appears when the energy of the plasma cycle reaches about 20 J, producing droplets at the filler wire of about 5.2 mg. Above this level, some drops are detached before the short-circuit, due to the gravity forces and Lorentz forces. This energy level of 20 J corresponds to the energy estimated by Lu et al. [23] for the droplets separation from a 1.2 mm diameter aluminium filler wire in GMAW with an arc current between 100 and 240 A. The standard deviation for the width is the lowest (around 0.1 mm) when the pulse duration is between about 1 and 2 ms (Figure 14(b)).

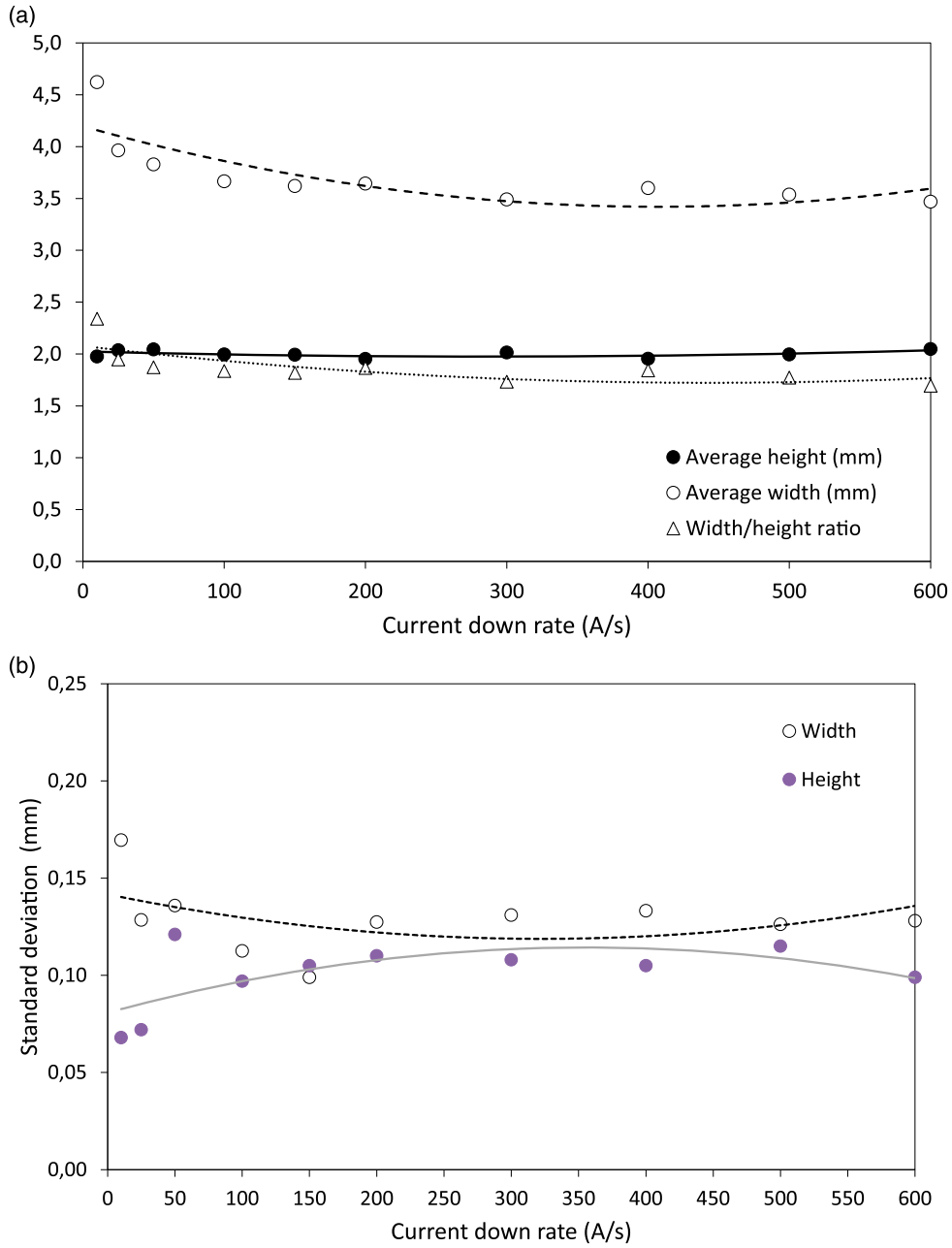


**Figure 15.** (a) Evolution of the average width and height of the deposits, and (b) of their standard deviation versus the current down rate.

The rate of the current decrease after the boost phase ($D_{boostdown}$) also modifies greatly the energy of the boost phase. If its value is low, the current remains at a high value during the wait phase, increasing the melting of the filler wire tip. That's why a too low value of this parameter produces an unstable transfer, as when the $I_{boost}$ or $t_{boost}$ increases. For values between 10 and 600 A ms$^{-1}$, the CMT transfer cycle is stable. The average height of the deposits remains rather constant, whereas the average width increases for the lowest values of $D_{boostdown}$, indicating a better wetting of the molten metal due to a higher energy of the plasma phase (Figure 15(a)). The standard deviation is minimal in the range 100–200 A ms$^{-1}$ (Figure 15(b)).

### *Wait phase current*

The wait current value controls the evolution of the drop during the feeding of the wire up to the short-circuit phase. If its value is too low (below 40 A), the wire tip partially solidifies during its feeding, and the deposit is un-regular (Figure 16). If its value is too high, above 100 A, the drop volume at the wire tip increases during the feeding, producing sometimes the drop detachment, spatters and un-regular deposits. A rather regular deposit can be then obtained when the wait current is in the 40–100 A range. However, the minimal standard deviation for the bead width is obtained for wait current between 40 and 70 A (Figure 16).

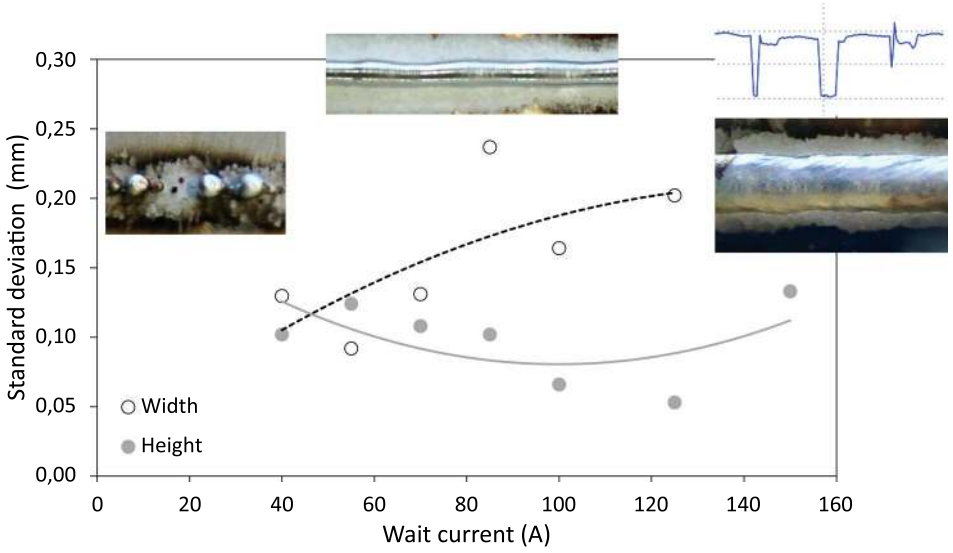


**Figure 16.** Evolution of the width and height standard deviations of the deposits versus the wait current, and aspect of the deposit, showing discontinuous beads when the wait current is too low and unstable metal transfer when the wait current is too high.

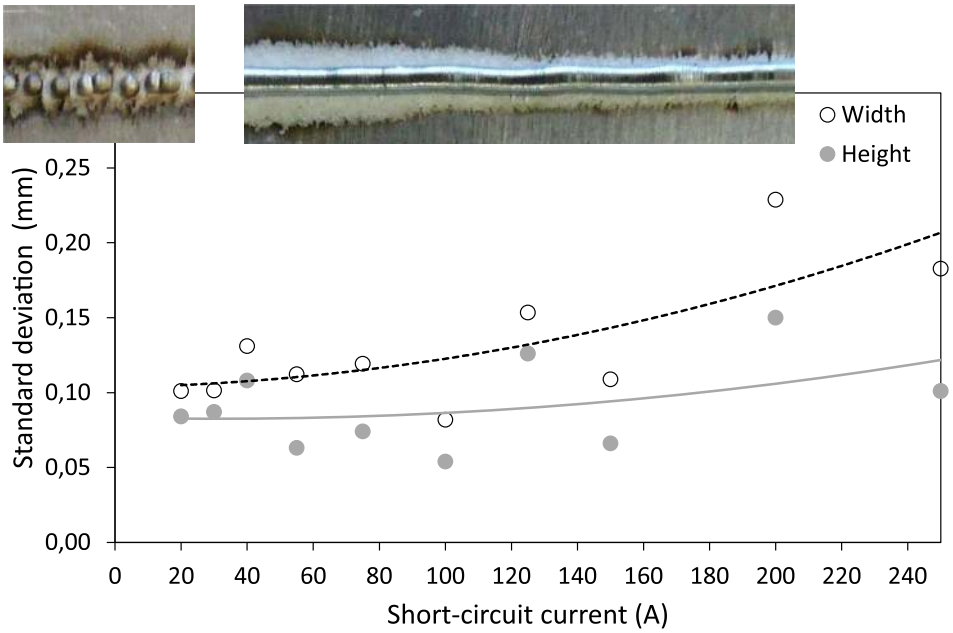


**Figure 17.** Evolution of the width and height standard deviations of the deposits versus the short-circuit current, and aspect of the deposit, showing discontinuous beads when the short-circuit current is too low.

### *Short-circuit current*

A minimal value of 20 A is needed for the short-circuit current to obtain a continuous deposit. Below this value, the bead forms separated solidified drops (Figure 17). This indicates the heating by joule effect during the short-circuit phase is important to avoid the rapid solidification of the wire tip when it touches the substrate surface. Above this value, the bead remains regular up to 150 A. For higher short-circuit current, the deposits are irregular. The standard deviation for the width is optimal, at about 0.1 mm, for short-circuit current between 20 and 100 A. Note that between 20 and 150 A, the bead geometry does not change drastically, the deposit height remains constant, and only the width slightly increases between 3.2 and 3.9 mm.

### *Feeding rate*

The feeding rate during the wait phase controls the duration of the wait phase, and then the deposit frequency of the droplets. A feeding rate below 10 m $min^{-1}$ produces a discontinuous deposit, the frequency of drop deposit being insufficient to guaranty the continuity of the molten metal (Figure 18). For instance, with a feeding rate of 5 m $min^{-1}$, less than 3 drops per second are deposited, corresponding to one drop each 5 mm of bead, which is clearly not enough to

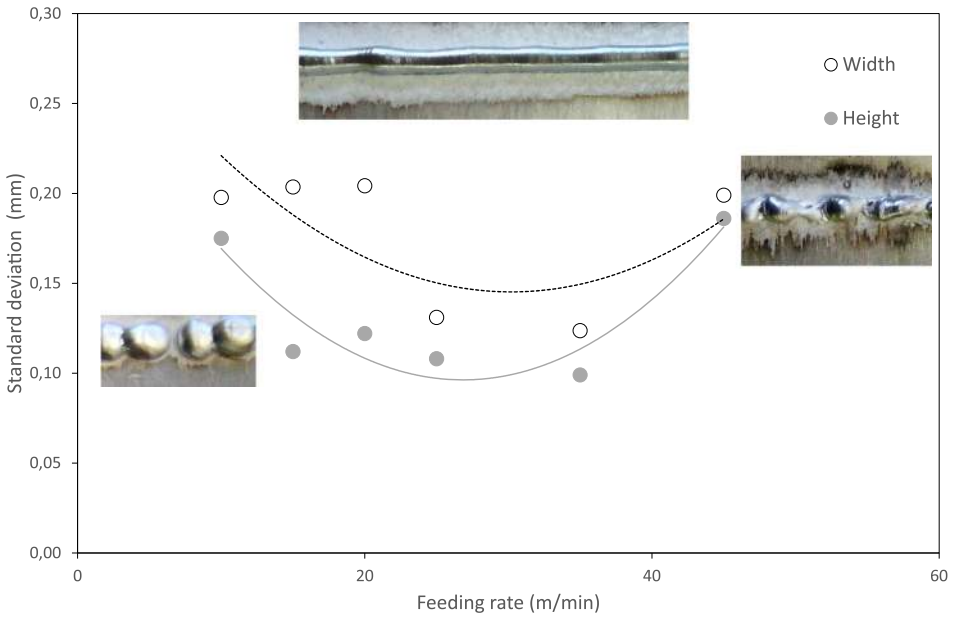


**Figure 18.** Evolution of the width and height standard deviations of the deposits versus the feeding rate, and aspect of the deposit, showing discontinuous beads when the feeding rate is too low or too high.

**Table 3.** CMT parameters ranges allowing to minimise the geometric standard deviation for width and thickness of deposited layers, and example of optimal parameters set for building AlSi5 shell structures.

| | $I_{wait}$ (A) | $V_d$ (m min$^{-1}$) | $I_{sc}$ (A) | $D_{boostup}$ (A ms$^{-1}$) | $T_{boostup}$ (ms) | $I_{boost}$ (A) | $t_{boost}$ (ms) | $D_{boostdown}$ (A ms$^{-1}$) |
|---|---|---|---|---|---|---|---|---|
| Optimal range | 40–70 | 20–45 | 20–100 | 300 | 0.1 | 100–175 | 1–2 | 100-200 |
| Optimised set | 70 | 35 | 60 | 300 | 0.1 | 150 | 1.5 | 150 |

form a regular deposit. At the opposite, when the feeding rate is too high, the filler wire cannot decelerates after the contact between the wire tip and the bead, and the solid part of the filler wire is 'sticked' to the substrate, making difficult its detachment. That also forms discontinuities on the bead, with some lake of material in some area corresponding to the zone of sticking of the filler wire (Figure 18). However, for feeding speed between 10 and 45 m min$^{-1}$, a continuous bead can be obtained. The best regular bead is obtained with feeding speed of about 35 m min$^{-1}$, giving a standard deviation of about 0.1 mm. The parameters range allowing to deposit walls with a good geometrical accuracy, and a choice of optimised parameters set for building shell structures are given in Table 3.

## Conclusion

A 3D print device has been developed to build shell shape aluminium parts by the WAAM process using a CMT welding station.

First tests using standard parameters pre-recorded in the welding station allowed to deposit monolayers with a geometrical accuracy, estimated according to the calculation of standard deviations of the height and the width of the bead measured on 50 cross sections, between 0.1 and 0.2 mm.

Multilayer deposits forming vertical walls by the addition of up to 100 layers are also obtained, with a width accuracy evaluated by the standard deviation of width measured on all the wall of about 0.3 mm. The building of multilayer walls required a progressive increase of the travel speed to keep a constant layer width, due to the heat accumulation during the addition of several layers. A linear increase of the wall height with the layer number has been reached, which is a promising result for additive manufacturing of aluminium parts, as the slicing of the part is generally achieved using a constant thickness for each layer.

Finally, a parametric study is achieved, in order to improve the geometrical accuracy by optimising the process parameters, changing their values from the standard ones. The results allow to understand the effect of the main process parameters controlling the arc current or voltage and the wire feeding on the metal transfer, and to give recommendations to improve the geometrical accuracy in order to obtain more regular walls, constituting basis for future manufacturing optimisation of real shell shape parts.

## Disclosure statement

No potential conflict of interest was reported by the authors.


## Funding

The authors are grateful to Conacyt for financial support of this work.



## ORCID

*S. Rouquette* http://orcid.org/0000-0002-1849-6142

## References


[1] Frazier WE. Metal additive manufacturing: a review. J Mater Eng Perform. 2014;23:1917–1928.

[2] Kannan GB, Rajendran DK. A review on status of research in metal additive manufacturing. In: Wimpenny DI, Pandey PM, Kumar LJ, editors. Advances in 3D printing & additive manufacturing technologies. Singapore: Springer Singapore; 2017. p. 95–100.

[3] Rashid R, Masood SH, Ruan D, et al. Effect of scan strategy on density and metallurgical properties of 17-4PH parts printed by Selective Laser Melting (SLM). J Mater Process Technol. 2017;249:502–511.

[4] Guo C, Ge W, Lin F. Effects of scanning parameters on material deposition during electron beam selective melting of Ti-6Al-4V powder. J Mater Process Technol. 2015;217:148–157.

[5] Ding D, Pan Z, Cuiuri D, et al. Wire-feed additive manufacturing of metal components: technologies, developments and future interests. Int J Adv Manuf Technol. 2015;81:465–481.

[6] Thompson SM, Bian L, Shamsaei N, et al. An overview of direct laser deposition for additive manufacturing; part I: transport phenomena, modeling and diagnostics. Addit Manufact. 2015;8:36–62.

[7] Jhavar S, Jain NK, Paul CP. Development of microplasma transferred arc (-PTA) wire deposition process for additive layer manufacturing applications. J Mater Process Technol. 2014;214:1102–1110.

[8] Lin J, Lv Y, Liu Y, et al. Microstructural evolution and mechanical property of Ti-6Al-4V wall deposited by continuous plasma arc additive manufacturing without post heat treatment. J Mech Behav Biomed Mater. 2017;69:19–29.

[9] Geng H, Li J, Xiong J, et al. Optimization of wire feed for GTAW based additive manufacturing. J Mater Process Technol. 2017;243:40–47.

[10] Williams SW, Martina F, Addison AC, et al. Wire+Arc additive manufacturing. Mater Sci Technol. 2016;32:641–647.

[11] Williams SW, Martina F. Wire+arc additive manufacturing vs. traditional machining from solid: a cost comparison. Technical report. Welding Engineering and Laser Processing Centre, Cranfield University; 2015.

[12] Wang P, Hu S, Shen J, et al. Characterization the contribution and limitation of the characteristic processing parameters in cold metal transfer deposition of an Al alloy. J Mater Process Technol. 2017;245:122–133.

[13] Feng J, Zhang H, He P. The CMT short-circuiting metal transfer process and its use in thin aluminium sheets welding. Mater Des. 2009;30:1850–1852.

[14] Pickin CG, Williams SW, Lunt M. Characterisation of the cold metal transfer (CMT) process and its application for low dilution cladding. J Mater Process Technol. 2011;211:496–502.

[15] Mezrag B, Deschaux-Beaume F, Benachour M. Control of mass and heat transfer for steel/aluminum joining using cold metal transfer process. Sci Technol Weld Join. 2015;20:189–198.

[16] Pang J, Hu S, Shen J, et al. Arc characteristics and metal transfer behavior of CMT+P welding process. J Mater Process Technol. 2016;238:212–217.

[17] Gu J, Cong B, Ding J, et al. Wire + arc additive manufacturing of aluminium. Proceedings of Solid Freeform Fabrication Symposium; 2014; Austin, USA. 451p.

[18] Chen M, Zhang D, Wu C. Current waveform effects on CMT welding of mild steel. J Mater Process Technol. 2017;243:395–404.

[19] Hu S, Zhang H, Wanga Z, et al. The arc characteristics of cold metal transfer welding with AZ31 magnesium alloy wire. J Manuf Process. 2016;24:298–306.

[20] Baoqiang C, Ruijie O, Bojin Q, et al. Influence of cold metal transfer process and its heat input on weld bead geometry and porosity of aluminum-copper alloy welds. Rare Met Mater Eng. 2016;45:606–611.

[21] Kumar NP, Vendan SA, Shanmugam NS. Investigations on the parametric effects of cold metal transfer process on the microstructural aspects in AA6061. J Alloys Compd. 2016;658:255–264.

[22] Gungor B, Kaluc E, Taban E, et al. Mechanical and microstructural properties of robotic Cold Metal Transfer (CMT) welded 5083-H111 and 6082-T651 aluminium alloys. Mater Des. 2014;54:207–211.

[23] Lu F, Wang HP, Murphy AB, et al. Analysis of energy flow in gas metal arc welding processes through self-consistent three-dimensional process simulation. Int J Heat Mass Transfer. 2014;68:215–223.